

# A Cast Copper Rotor Induction Motor for Small Commercial EV Traction: Electromagnetic Design, Analysis, and Experimental Tests

Qian Zhang, Huijuan Liu, *Member, IEEE*, Zhenyang Zhang and Tengfei Song

**Abstract**—According to the demands of the small commercial electric vehicle (EV) traction driving system, an 18kW inverter-driven induction motor (IM) with a die-casting copper squirrel cage rotor for traction drive was designed and evaluated. The 2D finite element model of the designed IM was built by considering the nonlinearity of core materials, and the geometric parameters of the motor were optimized. The operational performance of torque versus speed characteristics and the efficiency over the speed range under the rated (continuous) and overload condition were investigated. Finally, the designed inverter-driven IM was developed and the performance of the IM operating in three typical modes were tested respectively. The experimental results of the designed motor operating in various driven mode were compared with that of 2D FEM. All the results proved that the designed inverter-driven IM could meet the target specification of the small commercial EV.

**Index Terms**—Casting copper rotor, electric vehicle(EV), FEM, IM.

## I. INTRODUCTION

**D**UE to growing air pollution in urban areas, global warming caused by greenhouse gases as well as limited resources of fossil energy, and environmental protection was paid more attention, development of electric vehicles (EVs) have become a hot topic in automobile industry and some fields of transportation applications, e.g. forklifts, golf carts trolley bus and so on, around the world [1-3]. Although EVs suffer from issues such as a limited driving range due to the lower energy storage density of batteries compared with gasoline, and taking more time for batteries charging compared with gasoline filling. With rapid development of lithium ion batteries and the infrastructure popularization of charging station, EV would become be the best and ultimate solution.

Technology development for EV motors which form the core energy conversion components has gone a long way and progressed tremendously within the last two decades [4-7]. However, a typical EV motor still suffers from several key issues such as torque density in terms of weight and volume;

region of torque-speed capability; energy efficiency; reliability; and costs in manufacturing and maintenance. Currently, EVs are often equipped with induction motors (IMs) or interior permanent magnet synchronous motors (IPMs) [8-9].

IPM motor is considered to have a higher torque density, higher power density and higher efficiency with respect to IMs. However, in order to achieve much larger overload torque over the speed range [10], a safer back electromotive force (EMF) of high speed uncontrolled generator operation [11] and little sensitivity to PM temperature, the rotor of the IPM must be designed with multiple flux barriers for having a high saliency, which might look complicated industrial wise. In addition, the permanent magnet has the risk of demagnetization, and the costs of permanent magnet material and manufacturing of IPMs are higher than that of IMs.

IMs are adopted for their simple structure, high reliability, ruggedness, and universal availability, and the field-oriented vector control strategy is considered as an industrial standard. Moreover, IMs are naturally de-excited under the condition of inverter fault, and this is an important reason that extremely welcome among EV manufacturers, for safety.

The squirrel cage rotor of induction motor is usually built with aluminum bars or copper bars. Die-casting of the squirrel cage is a manufacturing technology, which can make the cage bars directly connected to the end rings. The manufacturing technology of aluminum die-casting rotor cage can be dated back to 1916 [12]. The manufacturing technology of copper die-casting rotor cage increased the costs of IM for a manufacturer because of the high melting point of copper which made the die life significantly short in the past. Recent researches improved the copper die-casting manufacturing technology and some products for improving the motor efficiency are now on the market [13-16].

According to the demands of the small commercial EV traction driving system, an 18kW inverter-driven IM with cast copper rotor was designed, a 2D finite element model of the motor, which considered the nonlinearity of the core material, was investigated. The geometric parameters of the motor, such as the width of slot opening, air gap length and slot skewed, were optimized. The torque versus speed characteristics and the efficiency of the whole speed range were calculated by 2D FEM. Finally, prototype motor was developed and the performance testing was completed on the experimental

Manuscript was submitted for review on 24, April, 2018.

Qian Zhang, Huijuan Liu, Zhenyang Zhang, and Tengfei Song are with the School of Electrical Engineering, Beijing Jiaotong University, Beijing, 100044 China (e-mail: qianzh@bjtu.edu.cn, hjliu@bjtu.edu.cn, 16117375@bjtu.edu.cn, 15121467@bjtu.edu.cn).

Digital Object Identifier 10.30941/CESTEMS.2018.00053

platform. The performance when the designed IM operating in various driven mode simulated by FEM was then verified by experimental results to confirm the validity of the methods.

## II. TRANSMISSION SYSTEM OF VEHICLE

The basic configuration of the transmission system for small commercial EV is shown in Fig.1. The wheels are driven by an IM through a transmission, and the IM of electric vehicle is driven by lithium batteries through DC-AC inverter. In addition to normal traction, the IM can work in the state of power generation, the mechanical energy of light-load and the kinetic energy of braking could be regenerate and reuse for the characteristic of four quadrant operation of the converter, which can improve the energy efficiency, extend the driving range of the EV.

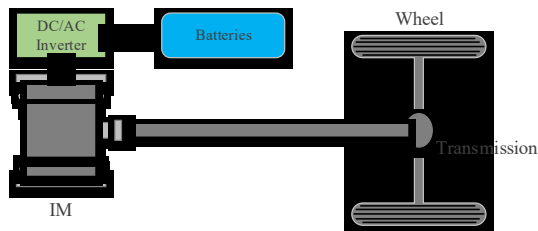


Fig. 1. Basic configuration of the transmission system for small commercial EV.

The torque characteristics of traction IM determine the vehicle running performance including vehicle acceleration, hill climbing ability and maximum speed. As shown in Fig.2, the actual torque characteristics curves of the small commercial EV traction motor contain rated and overload operation conditions. Both continuous curve (solid line) and overload (dashed line) curve have constant torque and constant power zones. It can be seen that EV requires a constant torque operating region to start and uphill march at low speed, while a constant power operating region at higher vehicle speed. The rated power  $P_1$  at maximum speed determines the maximum speed of the EV. The continuous torque  $T_1$  determines the maximum slope that the EV can climb continuously. Transient overload torque  $T_0$  is limited by the inverter current rating, and transient overload power is limited by the combination of voltage and current limits.

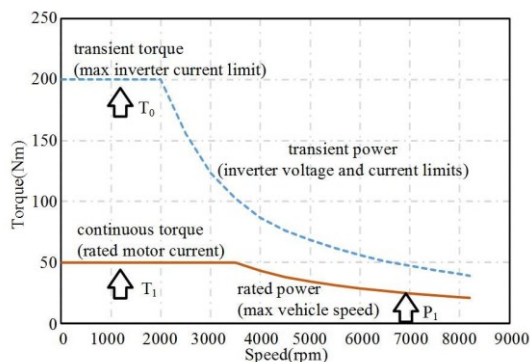


Fig. 2. The target specification of the small commercial EV.

The IM rated torque can be achieved by keeping a constant voltage-frequency ratio in the constant torque region. In this region, with the increase of supply voltage, the IM output

power increases linearly. Because the supply voltage magnitude is limited by the allowable maximum voltage provided, the voltage-frequency ratio is no longer constant even if the supply frequency keeps increasing at the corner speed, and then, the IM enters into the constant power operation region in which the motor current is constant while the air-gap flux reduces inversely proportional to the supply frequency, and the torque decreases inversely proportional to the speed of IM.

EVs are usually equipped with totally enclosed type motor in order to obtain better protection performance and prevent the external muddy water from damaging the EV motors. Due to the wide IM speed range and limitation of installation space, the cooling of motor designed in this paper is no longer dependent on the cooling fan on shaft, but on the aluminum alloy shell with the radiating rib of the motor which improves the cooling effect by the air flow in the motion of the EV. The equally distributed ventilation holes of rotor promote the cooling effect, and reduce the quality of IM.

## III. MOTOR DESIGN AND RESULTS

In general, the design of an induction motor is a complex process that requires electric machine theory, design experience, and many iterations and verifications. For the design of industrial IMs, standardized specifications relating to machine construction, cooling, safety, performance, testing and labeling which provided by industry and national or international standards should be met first.

### A. Difference between inverter-driven IM design and traditional IM

The inverter-driven IM design and the requirements of the motor performance are different from that of traditional IM [21]. For traditional IM, the starting torque, starting current, maximum torque, and the power factor and efficiency at the rated speed are the main concerns, as well as simple manufacture technology and low cost. However, for the IM used in variable voltage and variable frequency system, the design focuses on the power factor, efficiency and maximum torque, character of dynamic response, etcetera in the whole adjustable speed range.

In order to increase the starting torque, the rotor type of traditional IM is designed to be deep-slot or double cage type. The starting torque could be reached the maximum by lowering voltage and frequency if the magnetic flux remains constant when inverter-driven IM starts. Therefore, the rotor slot type of inverter-driven IM can be round-bottom, flat-bottom or closed type.

Generally, the negative influences of high-order harmonics from inverter should be considered in the course of inverter-driven IM design. High voltage climb ratio  $dv/dt$  produced by PWM is the menace to the winding insulation, which would shorten the life of the IM, even destroy the motor. Hence, the insulation should be improved so as to adapt the non-sinusoidal voltage. Moreover, additional losses, overheating, and over voltage caused by harmonics should be considered.

Specifically, the design of IMs includes 3 stages: 1) Choosing appropriate the pole number and slot numbers etc. 2)

Designing the motor dimensions and winding parameters to provide the required power at base speed within a specified space envelope. 3) Simulating the motor performance over its full speed range. Table I shows the specifications of the small commercial vehicle.

TABLE I  
THE SPECIFICATIONS OF THE VEHICLE

Item	Value
DC Voltage (V)	336
AC Voltage (V)	220
Power Rating $P_1$ (kW)	18
Current Rating (A)	62
Torque Rating $T_1$ (Nm)	50
Rating Efficiency (%)	94.0
Rating Power Factor	0.82
Rating Speed (rpm)	3500
Max Speed (rpm)	8200
Max Current@2000rpm (A)	200
Max Torque $T_0$ @2000rpm (Nm)	200
Max Power@2000rpm (kW)	42
Max Power@8200rpm (kW)	30
Motor Weight (kg)	<=60
Motor Size (mm×mm)	380×Φ265

### B. Stator and rotor design

The choice of pole number involves a compromise between machine weight and efficiency. Increasing the pole number reduces the flux per pole thereby the back-iron width can be reduced; however, the supply frequency must be higher and there will be greater harmonic content in the flux. The magnitude of the  $n$ 'th harmonic magnetomotive force (MMF) component is proportional to the  $n$ 'th harmonic winding factor and inversely proportional to  $n$ , thus the harmonic content of the stator MMF can be minimized by an appropriate choice of the stator slot number and coil pitch. 5/6 short pitch coefficient is adopted to reduce the high-order harmonics, and also the influence of additional torque produced by the 5th and 7th harmonics. In order to meet the space constraints imposed by the vehicle layout, the pole number of the drive motor is chosen for 4 and the stator winding is a double layer distribution type in 36 slots with a short-pitch of 8 slots.

A choice of the rotor slot number is necessary to alleviate the undesirable effects of harmonic fluxes such as, iron loss, noise and vibration. The rotor slot number is odd, which can reduce the synchronous parasitical torque, but also cause vibration by the magnetic unbalanced. Thus the even rotor slot number is chosen for high-speed inverter-driven IMs. For IMs under 100kW, rotor slots are straight while the stator slots are skewed can depress the electromagnetic noises. The iron losses of harmonics increase obviously even higher than the copper losses sometimes produced by the leakage flux effect of the skew rotor slots. The experimental results have been proved that the losses of IM with straight rotor slots are much less that of skew slots [21]. According to the empirical formulae have been proposed by [17], the rotor slots are straight and winding is a cast copper squirrel cage type with 44 bars. The semi-closed pyriform slot with round bottom is adopted on stator and the closed slot with round bottom is adopted on rotor as shown in Fig.3.

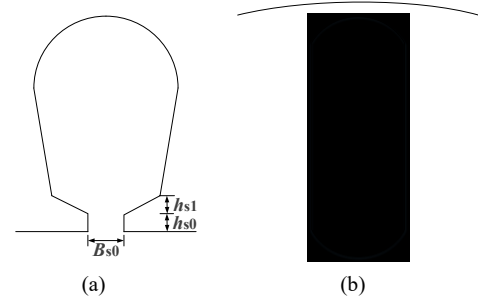


Fig. 3. Stator slot and rotor slot: (a) Stator slot; (b) Rotor slot.

### C. IM dimensions

It is known that the rated output of the motor is proportional to its volume, and the IM dimensions can be sized by using the so-called sizing equations:

$$D^2 l_{ef} = \frac{P' C_A}{n_N} \quad (1)$$

where  $D$  is the stator inner diameter in meters;  $l_{ef}$  is the axial length of motor in meters;  $P'$  is the computed output power of motor in kVA;  $n_N$  is the speed of motor in revolutions per second;  $C_A$  is machine coefficient.

The machine coefficient is defined by

$$C_A = \frac{6.1 \times 10^3}{\alpha_p' K_{wm} K_{dp} A B_\delta} \quad (2)$$

where  $\alpha_p'$  is the polar coefficient;  $K_{wm}$  is the waveform coefficient of air-gap flux density;  $K_{dp}$  is the winding factor;  $A$  is the electrical loading in amperes per meter;  $B_\delta$  is the magnetic loading in Tesla.

The sizing equation can be used to initiate the sizing process according to the specific needs and objectives. Then the electrical and magnetic loadings can be selected according to the reference or typical values provided in handbooks. For example, the electrical loading  $A$  depends on the cooling system and it typically correlates with shaft height.

Determining the air-gap length and the length of the motor involves more than pulling reference values from handbooks, as there are several things to consider, such as the possibility of fitting the required number of slots, cost, cooling behavior, inertia, etc. The air gap length  $g$  of the IM can be calculated by the following formula:

$$g = \frac{D}{1000} \left( 1 + \frac{9}{2^p} \right) \quad (3)$$

Where  $g$  is the air gap length in mm; and  $p$  is the pole pairs.

Constraints imposed by the geometrical standardization should be carefully taken into account in selecting diameter and length. For standard induction motors there are guidelines on how to choose the aspect ratio  $\lambda = l_{ef}/D$ , empirical sizing coefficients and approximate relationships to compute the diameter [17-19]. The designer should choose the most appropriate ratio for the specific application under consideration.

After sizing the main dimension and choosing the winding parameters of the proposed IM, the next stage for the IM design

should be based on the T-type equivalent circuit to provide the specified rated power at base speed; the parameters and performance of the motor are calculated during an iteration of the design process. After this, all performance of the motor may be simulated over the full speed range using a 2D time-stepping finite element method that models saturation, skin effect and nonlinearity of core materials are considered.

Totally enclosed type is adopted with the ingress protection IP67. It required that the maximum temperature rise of the motor is no more than 125K in continuous operation. The cooling of the IM is dependent on the distributed holes of rotor, and the aluminum alloy shell with the radiating rib of the motor cooled by the air flow in the motion of the EV.

By trial-and-error, the key design data of the IM listed in Table II are determined with the design specifications.

TABLE II  
THE MAIN DIMENSIONS OF THE IM

Quantity	Value
Pole number	4
Phase number	3
Slots per pole of each phase	3
Coil pitch in slot	8
Stator slot number	36
Rotor slot number	44
Stator outer diameter (mm)	220
Stator inner diameter (mm)	141
Rotor outer diameter (mm)	140
Rotor inner diameter (mm)	48
Air-gap length (mm)	0.5
Core stack length (mm)	143
Conductor number per phase	60
Conductor number per slot	10
Parallel branches number	2
Coil turns number	5
Electric load(A/cm)	248.791
Current density(A/mm <sup>2</sup> )	4.4389
Thermal load(A <sup>2</sup> /cm <sup>2</sup> ·mm <sup>2</sup> )	1104.36

#### IV. ELECTROMAGNETIC PERFORMANCE ANALYSIS

On the basis of considering the nonlinearity of the core material, the 2D finite element transient nonlinear model of the motor was established, and the reliability of the FEA software had been fully verified. The performance evaluation of the IM is based on the 2D FEM analysis by using the Maxwell 2D solvers. Fig.4a shows the 2D FEM model of the designed IM, and Fig.4b shows its mesh map. Considering the accuracy of the FEM results, the density of the mesh elements, especially in air-gap, must be sufficient. For this motor, the mesh in air gap between the stator and rotor is subdivided into 4 layers; the total elements number of the model is 20602. The ferromagnetic material of the stator and rotor core is the silicon steel sheet (35W300).

For an inverter-driven IM in an electric vehicle driving application, the values of various leakage reactance affect the motor performance, such as the desired speed range. In order to design a motor that meets the requirement, the effects of air gap length, stator slot opening width and slot skewed on the performance of the IM are investigated by using the 2D FEM simulation method.

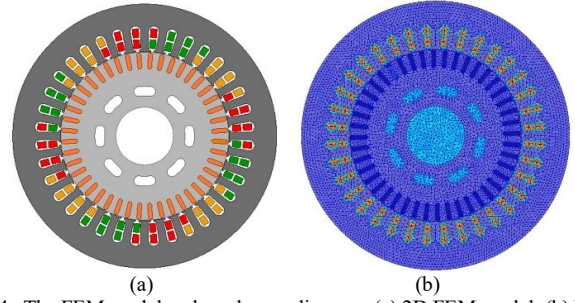


Fig. 4. The FEM model and mesh map diagram: (a) 2D FEM model; (b) Mesh map.

##### A. Air gap length

Air gap length has great influence on IM performance and operation reliability, and the following factors should be considered when determining its value: 1) In order to reduce excitation current and improve power factor, the air gap should be as small as possible; 2) The smaller the air gap, the larger the harmonic magnetic field and harmonic leakage reactance, the larger the stray loss and the higher the temperature rise. 3) In order to ensure the reliability of the motor and avoid the uneven air gap, the air gap cannot be too small. The air gap of the small motor should not be less than 0.25mm, and can be slightly adjusted on the basis of formula (3) according to the design requirements [18].

The efficiency at rated state versus air-gap length and the stator current at rated state versus air gap length of the motor can be computed and are shown in Fig. 5. It is noted that the stator current increases as the length of the air gap increases. From Fig.5, it can be found that the maximum efficiency of the IM can achieve 95% when the air gap length is 0.55 mm, and with this air gap length, the stator current is about 62.8A which exceeds its rated value 62A in table I. Therefore, in the sample motor design, the air gap length of 0.5mm is chosen.

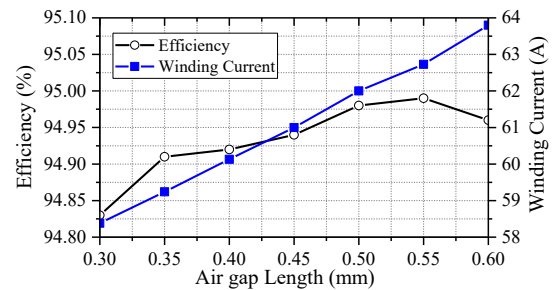


Fig. 5. The curves of efficiency and stator current versus air gap length.

##### B. Stator slot opening width

The semi-closed pyriform slot with round bottom is adopted on stator as shown in Fig.3, the use of this type of slot can raise the full rate of the slot, reduce the loss on the surface of the stator core and pulsating loss in the tooth, improve the power factor and prolong the life-span of press tool [17].

Increasing stator slot openings can reduce slot leakage but increases the harmonics of the teeth magnetic permeability which contribute to iron loss, noise and vibration. Generally, the width of stator slot opening  $B_{s0}$  is 2.5mm to 4mm, and

1.2mm-1.6mm larger than the glazed wire diameter of the coil for the purpose of stator winding embedding [17]. Fig.6 shows the harmonics magnitude of air gap flux density at different stator slot opening width  $B_{s0}$  with the same slot area, slot wedge and so on. It is noted that with the decrease of the stator slot opening width, the magnitudes of the 5th, 7th, 13th, 15th, 17th and 19th harmonics of the air-gap flux density are remarkably reduced. Because the wire diameter of the coil is 1.1mm, the opening width of stator slot can be 2.5mm.

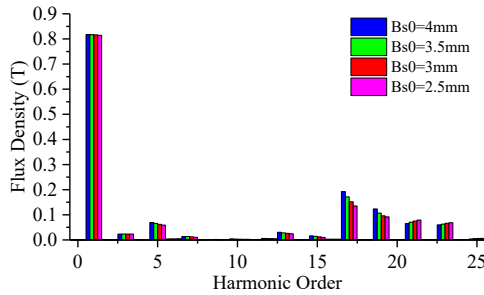
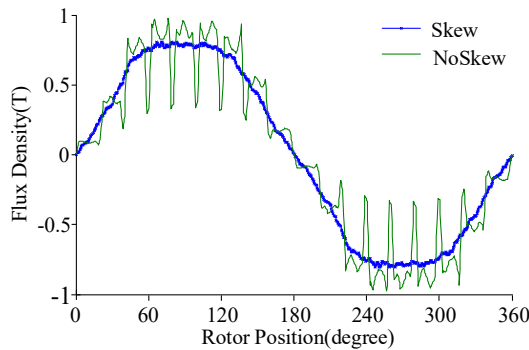


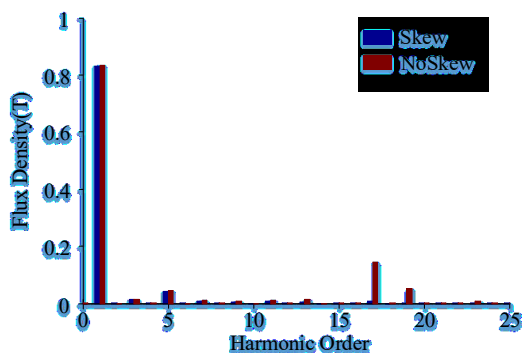
Fig. 6. The harmonics magnitude of air-gap flux density at different slot openings width.

C. Effect of slots skewed

Rotor slots are straight type in order to reduce the iron losses of harmonics, and to skew stator slots in inverter-driven IM can depress the electromagnetic noises [21]. The order of cogging harmonics  $v=2mq\pm 1$  of the air gap flux density are weakened when the slot skew distance is equal to one teeth pitch, in this paper, the skew mechanical angle is 10 degrees.



(a)



(b)

Fig. 7. The air-gap flux density waveform and its harmonics analysis: (a) Air-gap flux density waveform; (b) Harmonics analysis.

Slot skewed model and no slot skewed model are all built to

simulate the effects of slot skewed on air-gap flux density and its harmonics under rated load condition. Fig.7a shows the air-gap flux density waveform, when considering the slot skewed and no skewed respectively. Where the air-gap flux density waveform of slot skewed is the average value of the superposition of flux density on the axial direction with the 10 degree mechanical angle skewed. Fig.7b shows the harmonics amplitude of the flux density with slot skewed and no skewed. The 17th and 19th cogging harmonics existed in flux density are obviously suppressed by stator slot skewed.

D. Performance analysis

In order to meet the torque limitation and stator current limitation over the full speed range, the air gap length of the motor is 0.5mm, the stator slot opening width is 2.5mm, and the stator slot skew distance is 9.84mm, the skew mechanical angle is 10 degrees, which is one pitch of stator teeth. All of these options can reduce the harmonics of the motor and achieve a certain power factor of 0.83(lagging).

Fig. 8 shows the torque versus speed curve maps at full speed range by using 2D FEM simulation, and the efficiency maps at full speed range calculated by using 2D FEM are also reported in Fig.9. From Fig. 8 and Fig.9, it is noted that this IM can run safely at peak torque (200Nm), the efficiency of the motor in most of the operation areas are more than 90%, and the maximum efficiency can achieve 94.4% which has met the requirements of the manufacturer.

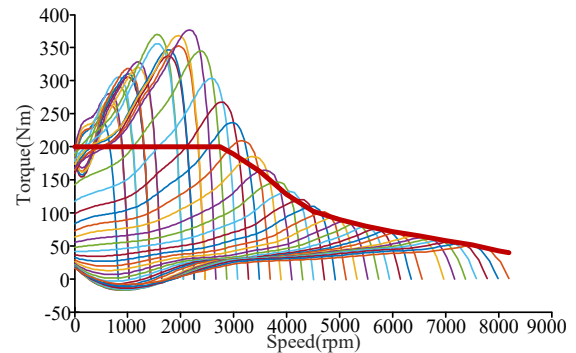


Fig. 8. The torque versus speed curve during all speed range.

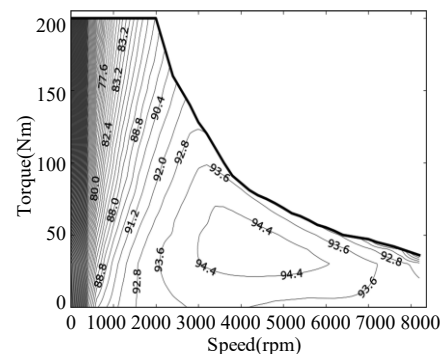


Fig. 9. Efficiency maps during full speed range.

Several key parameters of the designed IM calculated by using T-type equivalent circuit and 2D FEM when the motor working at rated speed mode, overload torque mode and maximum speed mode are summarized in Table III in order to compare with the experimental test results.

TABLE III  
COMPARISON OF SIMULATION RESULTS WITH TEST RESULTS

Items	T-circuit	2D FEM	Test
Rated speed @3500rpm	Line voltage(V)	220	221
	Phase current(A)	61.23	61.2
	Torque(Nm)	50.01	49.84
	Output power(kW)	18.33	18.27
	Speed(rpm)	3500	3500
	Total losses(kW)	1.065	0.9659
	Efficiency(%)	94.51	94.98
	Power factor	0.827	0.825
	0.7842		
Overload @2000rpm	Line voltage(V)	170	177.2
	Phase current(A)	189.5	218.3
	Torque(Nm)	200.5	199.5
	Output power(kW)	42	41.76
	Speed(rpm)	2000	2010.5
	Total losses(kW)	5.978	6.6025
	Efficiency(%)	87.54	86.35
	Power factor	0.8559	0.8233
	0.7642		
Max speed @8200rpm	Line voltage(V)	220	218.3
	Phase current(A)	106.94	118.7
	Torque(Nm)	36.59	31.29
	Output power(kW)	29.99	26.88
	Speed(rpm)	8200	8202.4
	Total losses(kW)	2.755	3.2
	Efficiency(%)	91.59	81.8
	Power factor	0.83	0.815
	0.7321		

V. EXPERIMENTAL VALIDATION

An 18kW, 4 poles, 220V inverter-driven IM with high efficiency has been designed and manufactured according to the main parameters of the motor as shown in table II. Fig. 10 shows the photograph of IM for small commercial EV. Where the distributed ventilation holes of rotor help to improve the heat dissipation and reduce the quality of the machine.

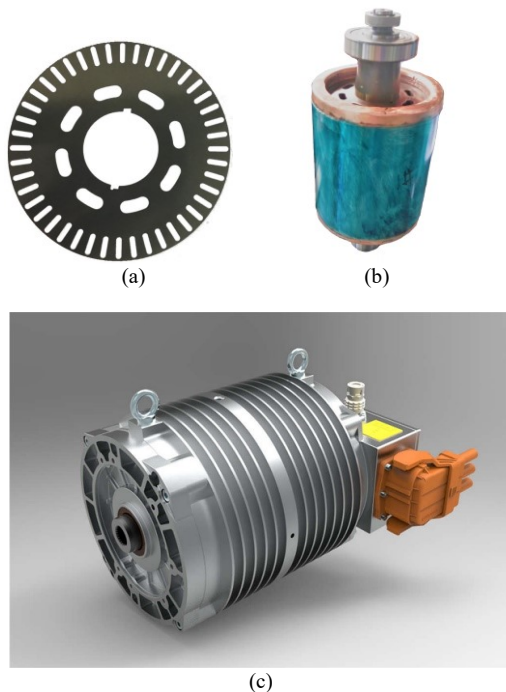


Fig. 10. 18kW IM photograph for EV: (a) Rotor core sheet; (b) Cast copper rotor; (c) Photograph of the prototype IM.

The experimental platform of the prototype was set up. Finally, the performance of the IM is evaluated based on the experimental tests as following: the test of start-up, locked rotor

and no-load; torque-power capabilities and energy efficiency over the designed speed-torque region; the performance of three kinds of operating mode about rated speed, overload torque, and max speed. Fig. 11 shows the experimental setup diagram and photograph of experimental platform.

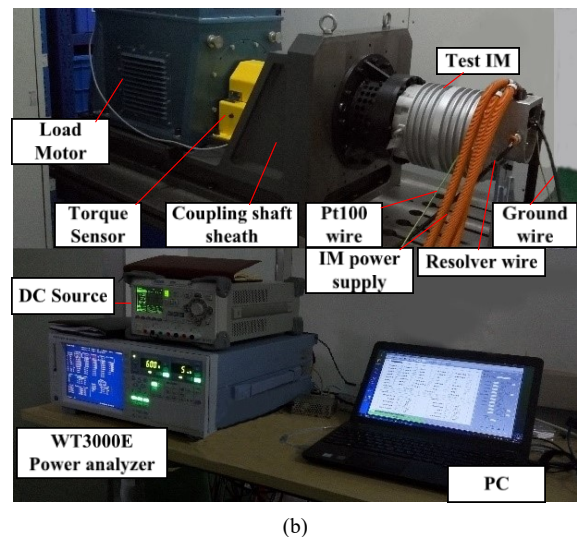
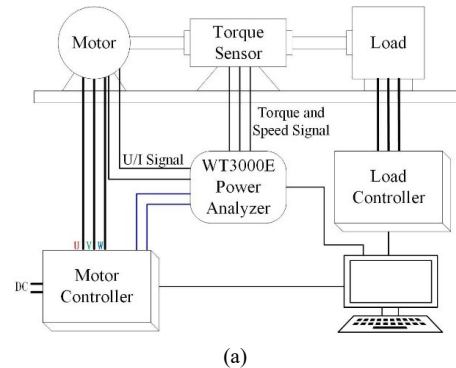
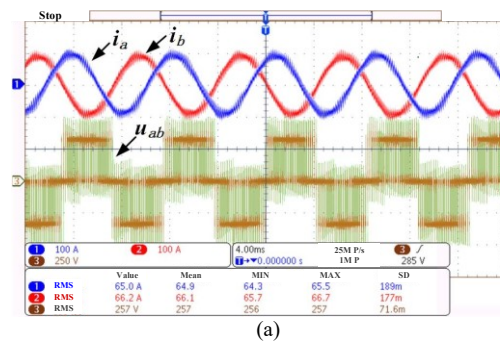


Fig. 11. Experimental setup diagram and photograph: (a) Experimental setup diagram; (b) Photograph of experimental platform.

In Figs. 12a, b and c, the recorded waveforms of current and voltage are shown when machine running at rated speed mode, overload torque mode and max speed mode respectively. The currents are in very good sine waveforms but contain some harmonics especially larger at overload torque and max speed condition. Therefore, the tested total losses of the IM running at these two operating condition are larger than the calculated results listed in Table III. The problem of tested total loss is larger than simulation total loss can be solved by improving the control method and reducing the harmonics of output voltage of the inverter.



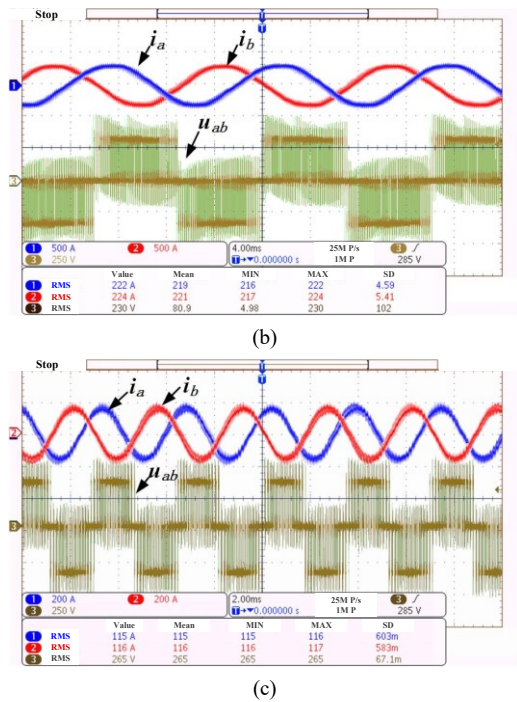


Fig. 12. Stator current and voltage waveforms at different running mode: (a) Rated speed mode; (b) Overload torque mode; (c) Max speed mode.

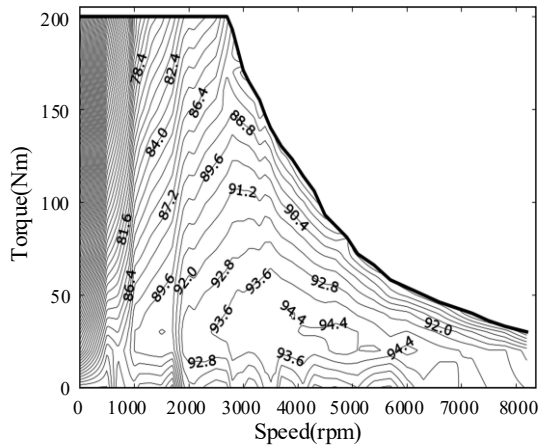


Fig. 13. Tested efficiency maps at full speed range.

For experimental testing about the power capabilities and energy efficiency, the testing efficiency in full speed range from 0 to 8200 rpm was examined, and as shown in Fig.13. It can be seen that the design results could reflect the tested efficiency maps in full speed range well as shown in Fig. 9, and both the maximum efficiency is 94.4%. Clearly shown in figure that the efficiency of the 75% operating points in the regime is higher than 90%, 60% operating points higher than 91%, and 35% operating points higher than 93%, including the rated operating points.

The comparison between the test results of several key parameters and the simulation results of the IM is listed in Table III. From table III, it also can be obtained that the design performance of rated speed mode calculated by using T-type equivalent circuit and 2D FEM of the motor agrees well with the experimental data of tests as a whole. Owing to the only one carrier frequency, the recorded currents contain some harmonics when the IM running at overload torque and max

speed, the tested total losses are larger than simulated total losses. The excitation of the machine windings was the standard sine wave when FEM and T-type equivalent circuit was used to calculate the power factor of the motor, while the IM was powered by inverter with the voltage of PWM in actual testing. The voltage and current measured by power analyzer including harmonics, which results in the higher test current and lower test power factor. These issues can be solved by improving the control method and reducing the harmonics of output voltage and current of the inverter. The other tested characteristics are in agreement with the simulated characteristics well when the IM running at overload torque and maximum speed mode. It can be confirmed that the 2D FEM could effectively simulate the performance and help designer to perform the analysis of the designed IM.

In addition to meeting the electromagnetic performance requirements, the designed inverter-driven IM for EV must also meet the strict requirements of noise, vibration and temperature rise. The temperature rise is 85.2K when the IM works continuously for 2 hours under rated condition. The acoustic noise and vibration of the motor and its system will be tested in a special laboratory and the analysis of thermal field, noise and vibration of the IM will be presented in detail in another paper.

## VI. CONCLUSION

According to the demands of the small commercial EV traction driving system, an 18kW inverter-driven IM with cast copper rotor was designed. Firstly, the approximate size of the motor was determined by the empirical formula and T-type equivalent circuit, and the performance of the rated operating condition was calculated and checked with the requirements. Then, the 2D finite element model of the designed IM, which considered saturation, skin effect, slot skewed and nonlinearity of core materials, was built. The geometric parameters of the motor were optimized, and the IM's operational performance of torque versus speed characteristics and the efficiency running at full speed range were simulated and investigated.

Finally, the designed inverter-driven IM was developed and the torque, speed, efficiency, power factor and so on of the IM operating in three typical modes were tested respectively. Besides, the efficiency maps over the speed range was drawn by testing. The experimental results of the designed motor operating in various driven mode were compared with that of simulation by FEM. All the results show that the designed inverter-driven IM can meet all requirements of the small commercial electric vehicle driving applications.

It is worth noting that when the specific performance involves saturation and complicated structures, the use of finite element method usually is the most potential method to meets the designer's aim.

## REFERENCES

- [1] M. Zeraouia, M. Benbouzid, and D. Diallo, "Electric motor drive selection issues for HEV propulsion systems: A comparative study," *IEEE Transactions on Vehicular Technology*, vol. 55, no. 6, pp. 1756-1764, Nov. 2006.
- [2] Z. Q. Zhu, and Q. Q. Chan, "Electrical machine topologies and technologies for electric, hybrid, and fuel cell vehicles," in *Proc. IEEE*

VPPC, Harbin, China, pp. 1-6, Sep. 2008.

- [3] I. Boldea, L. N. Tutelea, L. Parsa, and D. Dorrell, "Automotive electric propulsion systems with reduced or no permanent magnets: an overview," *IEEE Transactions on Industrial Electronics*, vol. 61, no. 10, pp. 5696-5711, Oct. 2014.
- [4] A. Emadi, Y. J. Lee, and K. Rajashekara, "Power electronics and motor drives in electric, hybrid electric, and plug-in hybrid electric vehicles," *IEEE Transactions Industrial Electronics*, vol. 55, no. 6, pp. 2237-2245, Jun. 2008.
- [5] F. L. Mapelli, D. Tarsitano, and M. Mauri, "Plug-in hybrid electric vehicle: modeling, prototype, realization, and inverter losses reduction analysis," *IEEE Transactions Industrial Electronics*, vol. 57, no. 2, pp. 598-607, Feb. 2010.
- [6] A. Y. Saber, G. K. Venayagamoorthy, "Plug-in vehicles and renewable energy sources for cost and emission reductions," *IEEE Transactions Industrial Electronics*, vol. 58, no. 4, pp. 1229-1238, Apr. 2011.
- [7] D. J. Thrimawithana, U. K. Madawala, "A novel matrix converter based bi-directional IPT power interface for V2G applications," in *Proc. IEEE IEC*, Manama, Bahrain, pp. 495-500, Dec. 2010.
- [8] Z. Q. Zhu, D. Howe, "Electrical machines and drives for electric, hybrid, and fuel cell vehicles," *Proceedings of the IEEE*, vol. 95, no. 4, pp. 746-765, Apr. 2007.
- [9] K. T. Chau, C.C. Chan, C. H. Liu, "Overview of Permanent-Magnet Brushless Drives for Electric and Hybrid Electric Vehicles," *IEEE Transactions Industrial Electronics*, vol. 55, no. 6, pp. 2246-2257, Jun. 2008.
- [10] G. Pellegrino, A. Vagati, P. Guglielmi, and B. Boazzo, "Performance comparison between surface-mounted and interior PM motor drives for electric vehicle application," *IEEE Transactions Industrial Electronics*, vol. 59, no. 2, pp. 803-811, Feb. 2012.
- [11] T. M. Jahns, V. Caliskan, "Uncontrolled generator operation of interior PM synchronous machines following high-speed inverter shutdown," *IEEE Transactions on Industry Applications*, vol. 35, no. 6, pp. 1347-1357, Nov/Dec. 1999.
- [12] P. L. Alger, R. E. Arnold, "History of Induction Motors in America," *Proceedings of the IEEE*, vol. 64, no. 9, pp. 1380-1383, Sep. 1976.
- [13] E. B. Agamloh, A. Cavagnino, "High efficiency design of induction machines for industrial applications," in *Proc. IEEE WEMDCD*, Paris, France, pp. 33-46, Mar. 2013.
- [14] K. J. Park, K. Kim, S. Lee, D. Koo, K. Ko; and J. Lee, "Optimal design of rotor slot of three phase induction motor with die-cast copper rotor cage," in *Proc. ICEMS*, Wuhan, China, pp. 61-63, Oct. 2008.
- [15] J. L. Kirtley, J. G. Cowie, E. F. Brush, D. T. Peters, and R. Kimmich, "Improving Induction Motor Efficiency with Die-cast Copper Rotor Cages," in *Proc. IEEE PESG*, Tampa, America, pp. 1-6, Jun. 2007.
- [16] Ashwin D, Ashok S, M. Dixit, and V. Chavan, "Design optimization of 15 kW, 2-pole induction motor to achieve IE4 efficiency level with copper die-casting," in *Proc. ICTAP Energy*, Kollam, India, pp. 98-102, Jun. 2015.
- [17] S. K. Chen, "Design of the Electrical Machines," 2<sup>nd</sup> ed., Beijing: *China Machine Press*, 2000, pp.231-237.
- [18] Z. G. Huang, F. L. Fu, "Handbook of small and medium sized rotating machines design," 2<sup>nd</sup> ed., Beijing: *China Electric Power Press*, 2014, pp.45-46.
- [19] G. Z. Huang, F. L. Fu, "Y2 series three-phase asynchronous motors technical manual," Beijing: *China Machine Press*, 2004.
- [20] D. Lin; P. Zhou, W. N. Fu, Z. Badics, Z. J. Cendes, "A Dynamic Core Loss Model for Soft Ferromagnetic and Power Ferrite Materials in Transient Finite Element Analysis," *IEEE Transactions on Magnetics*, vol. 40, no. 2, pp. 1318-1321, Mar, 2004.
- [21] H. Guan, Z. M. Zhao, S. Meng, and X. D. Wu, "Optimal design for inverter-driven induction motors," *Proceedings of the CSEE*, vol. 24, no.7, pp.194-199, Jul. 2004.
- [22] Zhao, N., and N. Schofield, "An improved induction machine design procedure for electric vehicle traction," in *Proc. PEMD*, pp.1-6, Apr. 2016.



**Qian Zhang** received the M.S. degree in electrical engineering from Beijing Jiaotong University, Beijing, in 2010. He is currently pursuing the Ph.D. degree in electrical engineering at Beijing Jiaotong University. His research interest includes the optimal design and analysis of novel permanent- magnet and linear machines.



**Huijuan Liu** received Ph. D. in Electrical Engineering from Beijing Jiaotong University in 2009 and received the B.S. degree and M.S. degree from Tianjin University in 1989 and 1994 respectively. Since December 2015, she has been a Professor with Beijing Jiaotong University. Her current research interests mainly focus on numerical methods of electromagnetic field computation, optimal design and control of high performance electrical machines and novel electrical motors, such as induction machine, doubly fed brushless machine, and permanent magnetic machine for wind power and other new power source development.



**Zhenyang Zhang** was born in Zhengyang, Henan Province, in 1989. He is a Ph. D. student in Electrical Engineering of Beijing Jiaotong University. His research interest is analysis, optimal design of new structure electrical machines, such as Vernier machine, flux-modulated motor and PM motor for direct-drive applications.



**Tengfei Song** was born in Shijiazhuang, Hebei Province. He received the M.S. degree in electrical engineering from Beijing Jiaotong University, Beijing, in 2018. His research interest includes the analysis, optimal design of new structure electrical machines, such as flux-modulated motor for direct-drive applications.